Effect of the sp^2 carbon phase on *n*-type conduction in nanodiamond films

Tomohiro Ikeda,[1] Kungen Teii,[1,a)] C. Casiraghi,[2] J. Robertson,[2] and A. C. Ferrari[2]
[1]*Department of Applied Science for Electronics and Materials, Interdisciplinary Graduate School of Engineering Sciences, Kyushu University, Kasuga, Fukuoka 816-8580, Japan*
[2]*Department of Engineering, University of Cambridge, Cambridge CB3 0FA, United Kingdom*

(Received 19 May 2008; accepted 12 August 2008; published online 7 October 2008)

Structural and electrical conduction properties of nitrogen-doped nanocrystalline diamond films are studied as a function of deposition temperature (T_D) in a microwave Ar-rich/CH_4 plasma with 30%N_2 addition. Hall- and Seebeck-effect measurements confirm *n*-type conduction for T_D above 1100 K. For T_D from 1100 and 1220 K, the electron concentration increases up to 10^{20} cm^{-3} and the electron mobility is in the range of 4–8 $cm^2\ V^{-1}\ s^{-1}$. For T_D above 1250 K, the mobility decreases to ~ 1 $cm^2\ V^{-1}\ s^{-1}$. Low conductivity films deposited at low T_D exhibit semiconductorlike thermal activation in the Arrhenius plots, while high conductivity films deposited at high T_D are almost temperature independent, indicative of quasimetallic conduction. The nitrogen concentration in the films is about 0.3 at. %, independent of T_D. As T_D is increased, the sp^2 content and order increase. This is responsible for the appearance of midgap states, their delocalization, and the larger distance between diamond grains. The high conductivity at high T_D is due to the amount and crystallinity of sp^2 carbon, rather than the nitrogen concentration. © *2008 American Institute of Physics*. [DOI: 10.1063/1.2990061]

I. INTRODUCTION

Fabrication of high conductivity *p*- and *n*-type diamond films is desired in order to use diamond as a core semiconductor material for high-frequency, high-power, low-loss, and environment conscious electronic devices.[1,2] The majority of works have so far focused on the development of doping techniques in homoepitaxial growth of diamond films.[3–5] *p*-type conduction has been obtained by substitutional incorporation of boron, which has an acceptor activation energy of 0.37 eV.[6] Hydrogen-terminated diamond surfaces have also been found to exhibit *p*-type conduction,[7] with lower activation energies ($\leq$ a few tens of meV).[8] *n*-type doping seems to be more difficult and problematic since substitutional incorporation of phosphorus has only been successful on (111)-oriented diamond with a donor activation energy of 0.6 eV,[9] and, hence, with a very low fraction of electron carriers activated at room temperature.[9] However, (111)-oriented diamond is not favored for device applications, since it is hard to polish. Recently, *n*-type doping of (100)-oriented diamond was reported with a donor activation energy of 0.58 eV.[10] It was also used to form a *p*-*i*-*n* junction giving high-efficiency deep ultraviolet (UV) emission.[11] However, the room-temperature conductivity of such *n*-type films, of the order of 10^{-5} and 10^{-7} $\Omega^{-1}\ cm^{-1}$ for (111)[9] and (100),[10] is much lower than rival materials, such as single crystal 4H-SiC (up to 10^3 $\Omega^{-1}\ cm^{-1}$),[12] due to the low doping efficiency of phosphorous and the high activation energy of electron carriers.[9,10] The research on diamond films with high *n*-type conductivity is thus of great interest for the application of diamond in power device technology.

A large effort is recently being made to intentionally grow nanocrystalline diamond films, also referred to as nanodiamond films.[13–21] A nanodiamond film is composed of three different carbon phases: the diamond phase in form of nanosized grains, *trans*-polyacetylene (TPA) segments, and amorphous carbon at the grain boundaries.[21] *n*-type conduction of nanodiamond has been reported by addition of N_2 to microwave Ar-rich/CH_4 plasmas.[22–24] In contrast to nitrogen-doped single crystal diamond with a donor activation energy of 1.7 eV,[25] nitrogen-doped nanodiamond films exhibit high conductivities even at room temperature, with an apparently low activation energy.[22–24] As nitrogen is preferentially incorporated into the amorphous carbon phase at the grain boundaries, new electronic states associated with carbon and nitrogen can be produced at and above the Fermi level.[26] This is wholly different from the formation of a single donor level beneath the conduction band minimum. High conductivities of nitrogen-doped nanodiamond films are due to their high electron concentration, of up to 10^{20}–10^{21} cm^{-3}.[22–24] In contrast, the electron mobility is between 1 and 10 $cm^2\ V^{-1}\ s^{-1}$,[22–24] comparable to amorphous silicon (0.1–10 $cm^2\ V^{-1}\ s^{-1}$),[27] and considerably higher than amorphous carbon films.[28–30] Electrical properties of nanodiamond films strongly depend on their structure. For instance, for a constant deposition temperature ($T_D \approx 1073$ K), the following has been observed: (i) electron concentration and conductivity increase exponentially with gas-phase N_2 concentration below 8 vol %, and saturate for further N_2 addition up to 20%;[22,24] (ii) electron mobility increases slightly with N_2 (10%–20%);[23,24] (iii) the sp^2/sp^3 ratio increases with N_2.[31,32] However, the relative contribution of sp^2-bonded carbon and incorporated nitrogen to the conduction still remains unclear.

In this paper, the properties of nitrogen-doped nanodiamond films are studied as a function of T_D. The structure of the amorphous carbon phase is expected to vary strongly

a)Author to whom correspondence should be addressed. Electronic mail: teii@asem.kyushu-u.ac.jp.

 © 2008 American Institute of Physics

Author complimentary copy. Redistribution subject to AIP license or copyright, see http://jap.aip.org/jap/copyright.jsp

with T_D because T_D promotes a transformation from sp^3- to sp^2-bonded carbon, thus increasing conduction. On the other hand, nitrogen introduction can also induce clustering,[33,34] increasing the conduction too. Here we try to separate these two effects.

II. EXPERIMENTAL

A modified AsTeX microwave plasma chemical vapor deposition apparatus with a quartz bell-jar reactor is used, as described previously.[35] Polished silica is utilized as substrate, since it is highly insulating, and, thus, suitable for measuring the film's electrical properties. Prior to deposition, the substrates are scratched with diamond powder diluted in ethanol in an ultrasonic generator and rinsed with de-ionized water to remove the excess powder residue. The substrates are then mounted on a grounded Mo holder equipped with a Ta wire heater and a water-cooling system. During deposition, the microwave power is kept at 800 W. The total pressure is monitored by a capacitance manometer and kept at 13.3 kPa. T_D at the substrate surface is monitored by an infrared pyrometer. The uncertainty of T_D is estimated within ± 15 K for a deposition area of 10×10 mm^2. T_D measured at the surface is about 30 K higher than that measured at the back, through the Mo stage, by a thermocouple. A mixture of $69\%Ar-30\%N_2-1\%CH_4$ (in vol %) is fed at a total flow rate of 200 SCCM (SCCM denotes cubic centimeter per minute at STP) from bottom of the reactor.

The films are examined by scanning electron microscopy (SEM), atomic force microscopy (AFM), x-ray diffraction (XRD) with 1.542 Å of Cu $K\alpha$ irradiation, and x-ray photoelectron spectroscopy (XPS) with 1486.6 eV excitation of Al $K\alpha$. Raman Spectroscopy is performed at 244 and 514 nm using two Renishaw Raman spectrometers optimized for UV and visible excitations, respectively. Note that p-type (100) Si, instead of silica, is used as the substrate for SEM and XPS to avoid charging effects. The film thickness is measured from step heights with a stylus profilometer. A four-point probe station in a van der Pauw geometry is used to measure Hall-effect coefficients at room temperature and the temperature dependence of the resistivity. The film thickness for the electrical measurements is in the range 0.6–1.7 μm. Four-point gold dot electrodes with 0.8 mm diameter are deposited on the films by vacuum evaporation. The Ohmic nature of the contacts is confirmed by measuring current-voltage characteristics.

III. RESULTS

SEM and AFM images of the films deposited on Si substrates at T_D=1020 and 1220 K are shown in Figs. 1(a)–1(d). For T_D below 1100 K, the films have smooth surface morphologies. As T_D increases above 1100 K, they develop ballaslike morphologies similar to lamellae, accompanied by a decrease in charging effects. For T_D above 1270 K, no film is deposited. The root-mean-square (rms) roughness estimated from the AFM images is 15.5 ± 2.5 nm for T_D=1020–1270 K, almost independent of T_D. The rms roughness is thus much bigger than in highly sp^3 amorphous carbons,[36,37] as expected in a nanocrystalline material. The growth rate in-

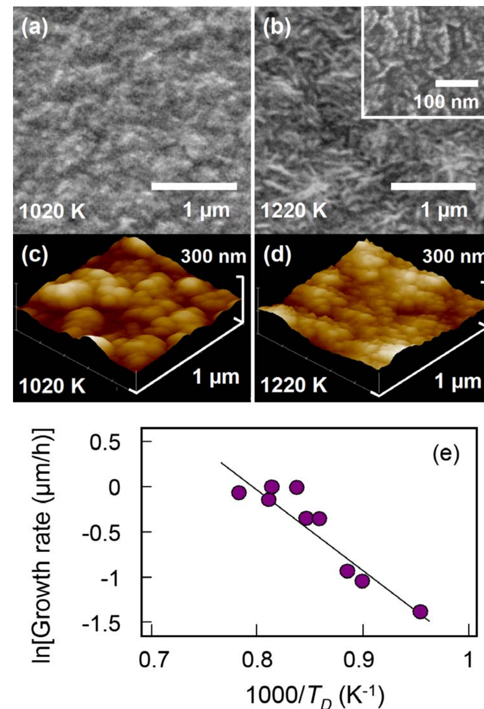

FIG. 1. (Color online) SEM and AFM images of the films deposited on silicon at [(a) and (c)] T_D=1020 K and [(b) and (d)] 1220 K. (e) Arrhenius plot of the growth rate of the films deposited on silica as a function of reciprocal T_D.

creases with T_D. The apparent activation energy (E_R) for the growth is calculated from the slope of the linear fit to the measured data in Fig. 1(e) by assuming an Arrhenius-type relation:

$$R = R_0 \exp\left(-\frac{E_R}{k_B T_D}\right), \quad (1)$$

where R is the growth rate, R_0 is the extrapolated value at $T_D\to\infty$, and k_B is the Boltzmann constant. The resulting $E_R=19\pm 3$ kcal/mol is more than twice the ~ 8 kcal/mol measured without N_2 addition in the same reactor.[35]

XRD patterns of the films deposited at various T_D are shown in Fig. 2. The intensity of each pattern is normalized by the typical amorphous halo at $2\theta\approx 22°$, arising from the

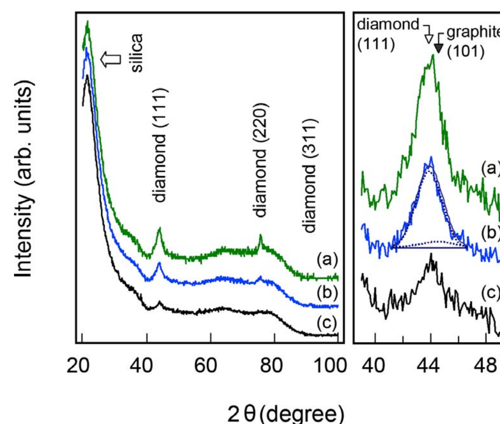

FIG. 2. (Color online) XRD patterns of the films deposited on silica at (a) T_D=1120, (b) 1220, and (c) 1270 K. Typical fits of the 2θ=43.9° and 44.6° peaks at 1220 K are given by dashed lines.

Author complimentary copy. Redistribution subject to AIP license or copyright, see http://jap.aip.org/jap/copyright.jsp

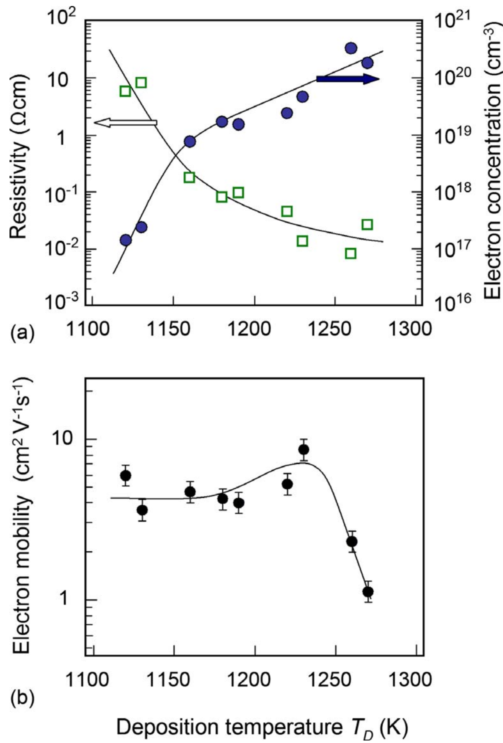

FIG. 3. (Color online) (a) Room-temperature resistivity and electron carrier concentration and (b) electron mobility of the films deposited on silica as a function of T_D.

silica substrate.[38] The diffractions from diamond {111} and {220} planes are observed at $2\theta=43.9°$ and $75.7°$,[39] respectively, while the diffraction from diamond {311} planes is much weaker. The overlap of the lonsdaleite {100} peak, normally at $2\theta=43.9°$,[39] with the diamond {111} peak is precluded since the primary {002} peak, normally at $2\theta=41.2°$, is absent. The contribution of the graphite {101} peak, normally at $2\theta=44.6°$,[39] is very small as shown in Fig. 2 by the relative intensity of the two Gaussian fitting curves. The apparent crystal size is calculated to be in the range of 10 ± 1 nm, independent of T_D, from the full width at half maximum (FWHM) of the diamond {111} peak, by using Sherrer's equation.[40]

The resistivity and electron concentration of the films at room temperature as a function of T_D are shown in Fig. 3(a). The error bar is $\pm20\%$. The films deposited at T_D below 1100 K are highly resistive with sheet resistivity of at least 10^6 Ω/sq ($\geq 10^2$ Ω cm for a 1 μm thickness film). Hall-effect measurement could not be carried out for them. The resistivity decreases exponentially by more than three orders of magnitude when T_D rises to 1200 K, and then saturates at $\sim10^{-2}$ Ω cm for further increase in T_D. Negative values of the Hall coefficients confirm that electrons are the majority carriers in these films. Electron concentration increases exponentially from 10^{17} to 10^{20} cm^{-3} with increasing T_D. The electron mobility of the films at room temperature as a function of T_D is shown in Fig. 3(b). The error bar is $\pm15\%$. The mobility is in the range 4–8 cm^2 V^{-1} s^{-1} for T_D between 1120 and 1220 K, and then shows a pronounced decrease down to ~1 cm^2 V^{-1} s^{-1} at the highest $T_D=1270$ K. The maximum values of the electron concentration and mobility

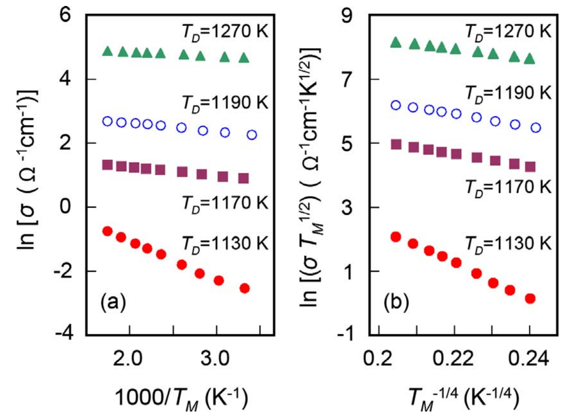

FIG. 4. (Color online) (a) Arrhenius plots of the conductivity σ of the films deposited on silica at various T_D as a function of reciprocal T_M and (b) dependence of $\sigma T_M^{1/2}$ on $T_M^{-1/4}$ for the data in Fig. 4(a).

are as high as those previously reported.[22–24] The n-type conduction of the films was also confirmed by Seebeck-effect measurements.

Arrhenius plots of the conductivity for the films deposited at various T_D are shown in Fig. 4(a). Measurements are done for sample temperature (T_M) ranging from room temperature up to 570 K. The dependence on T_M becomes smaller with increasing T_D. Thus, the low conductivity films deposited at low T_D exhibit thermal activation typical of semiconductors, while the high conductivity films deposited at high T_D show quasimetallic behavior. The apparent activation energy (E_σ) for the conduction is calculated from the slopes of the linear fit to the measured data in Fig. 4(a) by assuming

$$\sigma=\sigma_0 \exp\left(-\frac{E_\sigma}{k_B T_M}\right), \tag{2}$$

where σ and σ_0 are the conductivity and the extrapolated value at $T_M\rightarrow\infty$, respectively. E_σ decreases from 0.09 to 0.01 eV with increasing T_D from 1130 to 1270 K. However, the slopes for low T_D films are not fully linear in the entire T_M range and show a slight change at some T_M, depending on T_D. Electrical transport in nitrogen-doped nanodiamond films is considered to be a combination of thermal activation and hopping conduction of carriers in disordered grain boundaries.[26] Disordered materials often follow Mott-type variable-range hopping (VRH) if the density of states at the Fermi level is constant. In Fig. 4(b), the measured conductivity is replotted as a function of $T_M^{-1/4}$, according to Mott's three-dimensional VRH:[41]

$$\sigma=\sigma_{\text{VRH}} \exp\left[-\left(\frac{C}{T_M}\right)^{1/4}\right], \tag{3}$$

where σ_{VRH} is a prefactor and C is a material-dependent constant. Here we assume $\sigma_{\text{VRH}}=\sigma^0_{\text{VRH}}T_M^{-1/2}$, following Ref. 24, with σ^0_{VRH} independent of T_M. However, the slopes for low T_D films are not fully linear in the entire T_M range as in the case of the Arrhenius plots. Achatz *et al.*[24] suggested that the revised VRH model of Ref. 42 is more relevant to explain the temperature dependence of the conductivity.

Author complimentary copy. Redistribution subject to AIP license or copyright, see http://jap.aip.org/jap/copyright.jsp

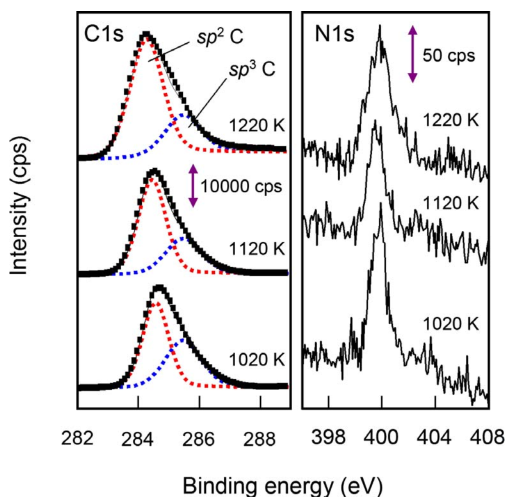

FIG. 5. (Color online) Core level C 1*s* and N 1*s* XPS spectra for the films deposited on silicon at T_D=1020, 1120, and 1220 K. Typical fits of the C 1*s* spectra are given by the dotted lines.

Core level C 1*s* and N 1*s* XPS spectra of the films deposited at various T_D are shown in Fig. 5. These are measured without surface sputtering since keV ion sputtering increases the amount of sp^2-bonded carbon by radiation damage.[43] Without N_2 addition, the N 1*s* peak is hardly observed. With N_2, the N 1*s* peak centered at 398.8–400.0 eV[44] appears with a low signal-to-noise ratio. The nitrogen concentration calculated from the integrated peak intensities by using the photoemission sensitivity factors is ~0.3 at. %, almost independent of T_D. This value remains constant after sputtering of several monolayers (1–2 nm). A near edge x-ray absorption study previously suggested that nitrogen in nanodiamond films is predominantly σ-bonded in the grain boundaries.[32] However, the assignment of nitrogen bonding environments by XPS is difficult because widely diverging reports are present for various nitrogen-incorporated amorphous carbons.[45,46] The C 1*s* peak position shows a downshift from 284.7 to 284.2 eV with T_D. After subtracting a Shirley background, each C 1*s* spectrum is decomposed by two fitting curves defined as 20% Lorentzian and 80% Gaussian distribution functions,[47] at 285.5 and around 284.4 eV for sp^3- and sp^2-bonded carbon.[48,49] The sp^3 peak is well fitted allowing the FWHM to vary at a fixed position, while the sp^2 peak has variable FWHM and position. The relative areas of the fits infer an increase of sp^2 content with T_D. The same trend has been shown for the dependence on N_2 concentration.[50]

Figures 6 and 7 show the visible and UV Raman spectra for the films deposited at various T_D. The visible spectrum (Fig. 6) shows four main bands at ~1150, 1350, 1450, and 1550 cm^{-1}. The peaks at 1350 and 1550 cm^{-1} are the *D* and *G* peaks, respectively. The *G* peak is due to the bond stretching of all pairs of sp^2 atoms in both rings and chains.[51] The *D* peak is due to the breathing modes of sp^2 atoms in rings and it is disorder activated.[51] The peaks at 1150 and 1450 cm^{-1} are signatures of the presence of TPA.[21] Their positions change with the excitation wavelength, depending on the conjugation length.[21] These peaks disappear for increasing temperature due to the release of hydrogen. The

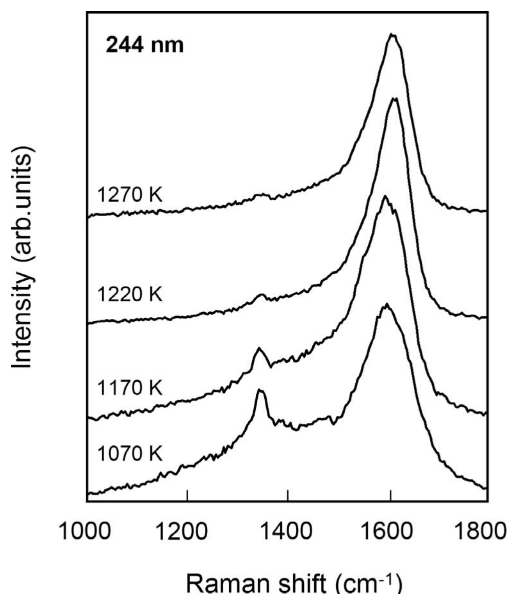

FIG. 6. UV Raman spectra with 244 nm excitation for the films deposited on silica at various T_D.

diamond peak is observed only in the UV spectrum. After subtracting a linear luminescence background, the spectra are fitted with four Lorentzians.

The main Raman fit parameters are as follows: the *G* peak dispersion [disp(*G*)], the ratio between the intensities of the *D* and *G* peaks [$I(D)/I(G)$], and the FWHM of the *G* peak [FWHM(*G*)]. The *G* peak dispersion is the variation of the *G* peak position measured at different excitation wavelengths.[21,33] This is defined here as[52]

$$\mathrm{disp}(G)(\mathrm{cm^{-1}/nm}) = [\mathrm{Pos}(G)@244 - \mathrm{Pos}(G)@514]/(514-244)\ \mathrm{nm}, \quad (4)$$

where Pos(*G*)@244 and Pos(*G*)@514 are the *G* peak positions measured at excitation wavelengths of 244 and 514 nm,

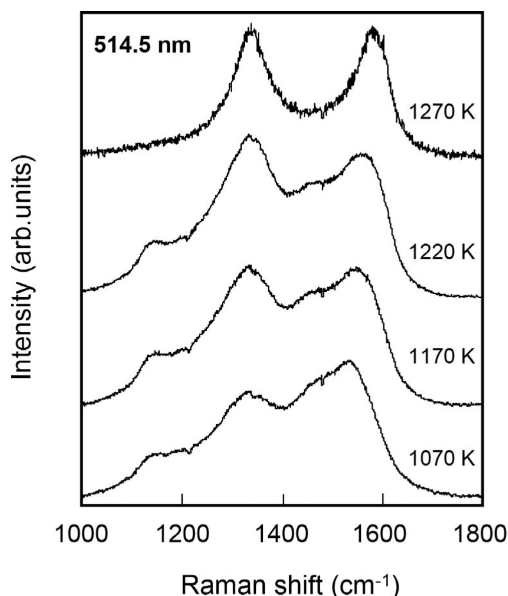

FIG. 7. Visible Raman spectra with 514.5 nm excitation for the films deposited on silica at various T_D.

Author complimentary copy. Redistribution subject to AIP license or copyright, see http://jap.aip.org/jap/copyright.jsp

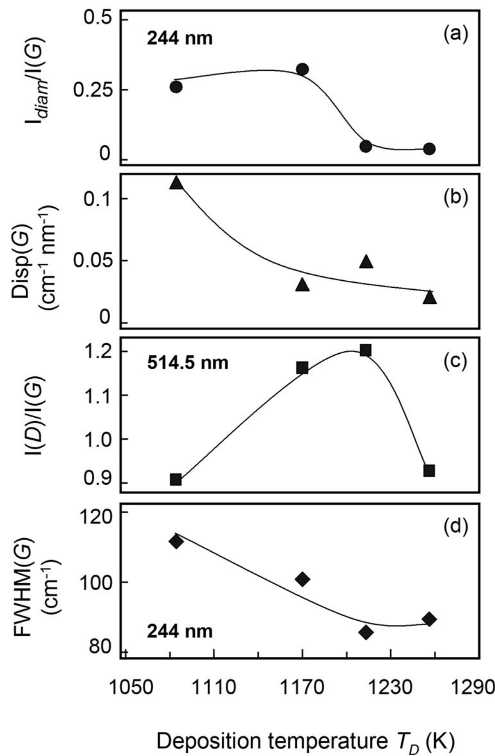

FIG. 8. (a) Intensity ratio of the diamond Raman peak to the G peak $[I_{\rm diam}/I(G)]$, (b) dispersion of the G peak, (c) $I(D)/I(G)$ ratio, and (d) FWHM of the G peak as a function of T_D.

respectively.[53] disp(G) probes the sp^2 configuration and its degree of disorder: a high disp(G) corresponds to a chainlike sp^2 configuration, while a low disp(G) corresponds to a ringlike sp^2 configuration.[21,53] The lower disp(G), the higher the ordering. $I(D)/I(G)$ measures the sp^2 cluster size: $I(D)/I(G)$ increases moving from graphite to nanocrystalline graphite, while it decreases moving from amorphous carbon to tetrahedral-amorphous carbon.[21] Finally, FWHM(G) is a probe of structural disorder: the higher FWHM(G), the higher the disorder.[21,53]

Figure 8 shows the evolution of the Raman fit parameters for increasing T_D: (i) the G peak dispersion decreases from 0.1 to 0 [Fig. 8(b)]; (ii) $I(D)/I(G)$ first increases and then decreases at the highest temperature [Fig. 8(c)]; (iii) FWHM(G), measured at 244 nm, decreases from ~120 to ~100 cm^{-1} [Fig. 8(d)]. These changes show that, by increasing temperature, we follow an ordering trajectory,[33,51] toward an almost fully sp^2 bonded phase, similar to nanocrystalline graphite. Figure 8(a) further shows that the relative intensity of the diamond peak to the G peak reduces from 0.3 to 0.04 with increasing T_D.

IV. DISCUSSION

According to Ref. 26, nitrogen atoms would be preferentially incorporated in the grain boundaries, as this is energetically favored. Doping would result from the formation of a number of midband states at and above the Fermi level: π and π^* states for sp^2-bonded atoms and σ^* states for sp^3-bonded atoms originating from the grain boundaries. These midband states form a spatially homogeneous band structure of delocalized states when the system is viewed as quantum size network of grains with grain boundaries. There are many configurations of nitrogen incorporation in sp^2-bonded carbon.[33] Many of them, in which nitrogen has a nonbonding lone-pair state, are not doping.[54] However, these midband states are not due to substitutional doping. The electron transport mechanism can be explained by VRH at localized states (or dangling bond states) near the Fermi level, when the conductivity is relatively low.[26] The quasimetallic behavior for the high conductivity films is more related to the π and π^* states.[26] Higher nitrogen concentrations in the films increase the relative amount of sp^2 carbon, resulting in an upward shift of the Fermi level, a broadening of the π and π^* states, and a strong delocalization of these states. These electronic changes are responsible for the increase in conductivity, similar to the case of nitrogen-doped amorphous carbon films.[54–58] Thus, rather than conventional doping, this reflects a nitrogen induced structural change.

In the present work, two T_D-dependent regions for conduction are observed: (i) for $1100 < T_D \leq 1220$ K, the electron concentration increases up to 10^{20} cm^{-3} and the mobility reaches 4–8 $\text{cm}^2\,\text{V}^{-1}\,\text{s}^{-1}$; (ii) for $T_D \geq 1250$ K, the mobility decreases to ~1 $\text{cm}^2\,\text{V}^{-1}\,\text{s}^{-1}$, while the electron concentration does not change. Since the nitrogen concentration measured by XPS remains almost constant at about 0.3 at. % and it is very low, the electrical properties must be related to the change in the amorphous carbon phase. XPS and Raman spectroscopy show an increase in the sp^2/sp^3 ratio and in the order of the sp^2 phase with T_D. The higher amount of sp^2 carbon increases the density of midband states associated with π bonding at and above the Fermi level. This raises the electron concentration, in agreement with the results in Fig. 3. Electron transport for the high conductivity films is governed by the localization of the π and π^* states in the grain boundaries and depends on two competitive processes. First, an increase in the spatial connectivity of sp^2-bonded carbon is expected from the rise in the relative amount of sp^2-bonded carbon. This causes a better overlap of the π electron orbitals among the sp^2 clusters and enhances the delocalization of the π and π^* states. This makes electron transport more probable and increases the electron mobility. Second, the concurrent decrease in the relative amount of diamond increases the mean distance between diamond grains. A spatially heterogeneous band structure is consequently formed. The system then behaves as grains and grain boundaries embedded in amorphous matrix. This lowers the electron mobility, as this is now limited by the low mobility of amorphous carbon (~10^{-6} $\text{cm}^2\,\text{V}^{-1}\,\text{s}^{-1}$).[28–30] A critical distance for this degeneration may be deduced from the localization length of carriers, which has been taken as 3 nm for similar highly conductive nanodiamond films in Ref. 24. The grain boundary thickness for the films in Ref. 24 is actually in the same range of ~2 nm or less.[31] The mobility remains constant when the two processes are balanced at low T_D, but decreases when the latter process becomes dominant at high T_D.

We now consider the relative contribution of sp^2 carbon and incorporated nitrogen to the conduction. Figure 9 shows the resistivity of our T_D=1100 and 1200 K films as a func-

Author complimentary copy. Redistribution subject to AIP license or copyright, see http://jap.aip.org/jap/copyright.jsp

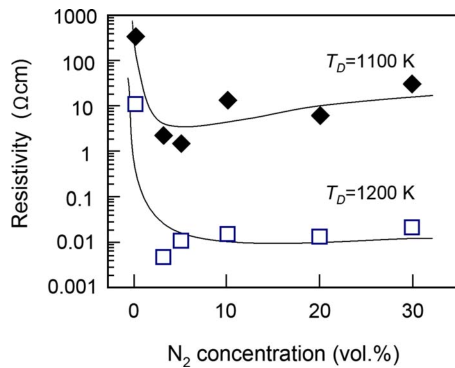

FIG. 9. (Color online) Room temperature resistivity of the films deposited on silica at $T_D=1100$ and 1200 K as a function of gas-phase N_2 concentration.

tion of gas-phase N_2 concentration. For both T_D, the resistivity decreases by two to three orders of magnitude upon 3%N_2 addition and saturates for further N_2 up to 30%. The minimum resistivity in the saturation region for each T_D becomes lower with T_D. The maximum nitrogen concentration measured by XPS is about 0.3 at. % for both T_D. This shows that the sp^2 phase is more responsible for increasing conduction than the nitrogen concentration itself.

Increasing ordering and amount of the sp^2 phase raises the electron concentration and lowers the resistivity, while the electron mobility stays constant. When the sp^2 phase becomes more crystalline, the resistivity slightly decreases and the electron concentration increases, but the mobility strongly decreases. This means that the sp^2 clustering is strongly affecting the electrical conduction properties of our films.

V. CONCLUSIONS

The properties of nitrogen-doped nanodiamond films were studied as a function of the deposition temperature T_D. For T_D between 1100 and 1220 K, the electron concentration exponentially increases up to 10^{20} cm^{-3} and the electron mobility is in the range of 4–8 $cm^2 V^{-1} s^{-1}$. Above 1250 K, the mobility decreases to ~1 $cm^2 V^{-1} s^{-1}$. The Arrhenius plots of the conductivity show a transition from semiconducting to quasimetallic conduction with increasing T_D. The nitrogen concentration in the films is about 0.3 at. %. Raman spectroscopy and XPS show that the amount and clustering of the sp^2 phase rise with increasing T_D, which explains the quasimetallic behavior for the high conductivity films.

ACKNOWLEDGMENTS

The authors thank Professor H. Nakashima for Hall-effect measurement. This research was supported by a Grant-in-Aid from the Ministry of Education, Science, Sports, and Culture of Japan. T.I. was supported by JSPS Research Fellowships for Young Scientists. K.T. acknowledges funding from the Iketani Science and Technology Foundation, the Kurata Memorial Hitachi Science and Technology Foundation, and the Japan-Taiwan Joint Research Program of Interchange Association, Japan. C.C. acknowledges funding from the Oppenheimer Fund. A.C.F. acknowledges funding from the Royal Society and the Leverhulme Trust.

[1] A. Denisenko and E. Kohn, Diamond Relat. Mater. **14**, 491 (2005).
[2] M. Kasu, K. Ueda, Y. Yamauchi, A. Tallaire, and T. Makimoto, Diamond Relat. Mater. **16**, 1010 (2007).
[3] S. A. Grot, C. W. Hatfield, G. Sh. Gildenblat, A. R. Badzian, and T. Badzian, Appl. Phys. Lett. **58**, 1542 (1991).
[4] S. Koizumi, M. Kamo, Y. Sato, H. Ozaki, and T. Inuzuka, Appl. Phys. Lett. **71**, 1065 (1997).
[5] I. Sakaguchi, M. N.-Gamo, Y. Kikuchi, E. Yasu, H. Haneda, T. Suzuki, and T. Ando, Phys. Rev. B **60**, R2139 (1999).
[6] G. Sh. Gildenblat, S. A. Grot, and A. R. Badzian, Proc. IEEE **79**, 647 (1991).
[7] M. I. Landstrass and K. V. Ravi, Appl. Phys. Lett. **55**, 975 (1989).
[8] O. A. Williams, M. D. Whitfield, R. B. Jackman, J. S. Foord, J. E. Butler, and C. E. Nebel, Appl. Phys. Lett. **78**, 3460 (2001).
[9] S. Koizumi, T. Teraji, and H. Kanda, Diamond Relat. Mater. **9**, 935 (2000).
[10] H. Kato, S. Yamasaki, and H. Okushi, Appl. Phys. Lett. **86**, 222111 (2005).
[11] T. Makino, N. Tokuda, H. Kato, M. Ogura, and H. Watanabe, S.-G. Ri, S. Yamasaki, and H. Okushi, Jpn. J. Appl. Phys., Part 2 **45**, L1042 (2006).
[12] H. K. Song, H. S. Seo, S. Y. Kwon, J. H. Moon, J. H. Yim, J. H. Lee, and H. J. Kim, J. Cryst. Growth **305**, 83 (2007).
[13] D. Zhou, A. R. Krauss, L. C. Qin, T. G. McCauley, D. M. Gruen, T. D. Corrigan, R. P. H. Chang, and H. Gnaser, J. Appl. Phys. **82**, 4546 (1997).
[14] D. Zhou, T. G. McCauley, L. C. Qin, A. R. Krauss, and D. M. Gruen, J. Appl. Phys. **83**, 540 (1998).
[15] K. Teii and T. Yoshida, J. Appl. Phys. **85**, 1864 (1999).
[16] K. Okada, S. Komatsu, and S. Matsumoto, J. Mater. Res. **14**, 578 (1999).
[17] X. T. Zhou, Q. Li, F. Y. Meng, I. Bello, C. S. Lee, S. T. Lee, and Y. Lifshitz, Appl. Phys. Lett. **80**, 3307 (2002).
[18] K. Teii, M. Hori, and T. Goto, J. Appl. Phys. **95**, 4463 (2004); K. Teii, Chem. Phys. Lett. **389**, 251 (2004).
[19] C. Popov, W. Kulisch, P. N. Gibson, G. Ceccone, and M. Jelinek, Diamond Relat. Mater. **13**, 1371 (2004).
[20] P. W. May, J. N. Harvey, J. A. Smith, and Yu. A. Mankelevich, J. Appl. Phys. **99**, 104907 (2006).
[21] A. C. Ferrari and J. Robertson, Phys. Rev. B **63**, 121405(R) (2001).
[22] S. Bhattacharyya, O. Auciello, J. Birrell, J. A. Carlisle, L. A. Curtiss, A. N. Goyette, D. M. Gruen, A. R. Krauss, J. Schlueter, A. Sumant, and P. Zapol, Appl. Phys. Lett. **79**, 1441 (2001).
[23] O. A. Williams, S. Curat, J. E. Gerbi, D. M. Gruen, and R. B. Jackman, Appl. Phys. Lett. **85**, 1680 (2004).
[24] P. Achatz, O. A. Williams, P. Bruno, D. M. Gruen, J. A. Garrido, and M. Stutzmann, Phys. Rev. B **74**, 155429 (2006).
[25] A. T. Collins and E. C. Lightowlers, in *The Properties of Diamond*, edited by J. E. Field (Academic, London, 1979), Chap. 3, pp. 79–105.
[26] P. Zapol, M. Sternberg, L. A. Curtiss, T. Frauenheim, and D. M. Gruen, Phys. Rev. B **65**, 045403 (2001).
[27] B. K. Choo, J. S. Choi, S. W. Kim, K. C. Park, and J. Jang, J. Non-Cryst. Solids **352**, 1704 (2006).
[28] W. Mycielski, E. Staryga, A. Lipinski, S. Mitura, and A. Sokolowska, Diamond Relat. Mater. **3**, 858 (1994).
[29] A. Foulani, C. Laurent, B. Mebarki, and Y. Segui, J. Appl. Phys. **80**, 470 (1996).
[30] L. Klibanov, M. Oksman, A. Seidman, and N. Croitoru, Diamond Relat. Mater. **6**, 1152 (1997).
[31] J. Birrell, J. A. Carlisle, O. Auciello, D. M. Gruen, and J. M. Gibson, Appl. Phys. Lett. **81**, 2235 (2002).
[32] J. Birrell, J. E. Gerbi, O. Auciello, J. M. Gibson, D. M. Gruen, and J. A. Carlisle, J. Appl. Phys. **93**, 5606 (2003).
[33] A. C. Ferrari, S. E. Rodil, and J. Robertson, Phys. Rev. B **67**, 155306 (2003).
[34] B. Kleinsorge, A. C. Ferrari, J. Robertson, and W. I. Milne, J. Appl. Phys. **88**, 1149 (2000).
[35] K. Teii and T. Ikeda, Appl. Phys. Lett. **90**, 111504 (2007).
[36] C. Casiraghi, A. C. Ferrari, R. Ohr, A. J. Flewitt, D. P. Chu, and J. Robertson, Phys. Rev. Lett. **91**, 226104 (2003).
[37] M. Moseler, P. Gumbsch, C. Casiraghi, A. C. Ferrari, and J. Robertson, Science **309**, 1545 (2005).

Author complimentary copy. Redistribution subject to AIP license or copyright, see http://jap.aip.org/jap/copyright.jsp

[38]W. Vogel, S. Botti, S. Martelli, and E. Carlino, New J. Chem. **22**, 749 (1998).
[39]JCDPS Powder Diffraction File Nos. ASTM 6-0675, ASTM 19-268, and ASTM 23-64, International Center for Diffraction Data Swarthmore, 1990.
[40]B. D. Cullity, *Elements of X-Ray Diffraction* (Addison-Wesley, Reading, MA, 1978).
[41]N. Mott, *Conduction in Non-Crystalline Materials* (Oxford Science, New York, 1987).
[42]C. Godet, J. Non-Cryst. Solids **299–302**, 333 (2002).
[43]M. S. Dresselhaus and R. Kalish, *Ion Implantation in Diamond, Graphite and Related Materials*, Springer Series in Materials Science Vol. 22 (Springer, Berlin, 1992).
[44]C. D. Wagner, W. M. Riggs, L. E. Davis, J. F. Moulder, and G. E. Muilenberg, *Handbook of X-Ray Photoelectron Spectroscopy* (Perkin-Elmer, Physical Electronics, Eden Prairie, MN, 1979).
[45]N. Hellgren, J. Guo, C. Såthe, A. Agui, J. Nordgren, Y. Luo, H. Ågren, and J.-E. Sundgren, Appl. Phys. Lett. **79**, 4348 (2001).
[46]S. E. Rodil and S. Muhl, Diamond Relat. Mater. **13**, 1521 (2004).
[47]T. Y. Leung, W. F. Man, P. K. Lim, W. C. Chan, F. Gaspari, and S. Zukotynski, J. Non-Cryst. Solids **254**, 156 (1999).
[48]S. Bhattacharyya, C. Cardinaud, and G. Turban, J. Appl. Phys. **83**, 4491 (1998).
[49]W. Lu and K. Komvopoulos, J. Appl. Phys. **85**, 2642 (1999).
[50]K. L. Ma, J. X. Tang, Y. S. Zou, Q. Ye, W. J. Zhang, and S. T. Lee, Appl. Phys. Lett. **90**, 092105 (2007).
[51]A. C. Ferrari and J. Robertson, Phys. Rev. B **61**, 14095 (2000); **64**, 075414 (2001).
[52]A. C. Ferrari, Surf. Coat. Technol. **180–181**, 190 (2004).
[53]C. Casiraghi, A. C. Ferrari, and J. Robertson, Phys. Rev. B **72**, 085401 (2005).
[54]A. Ilie, O. Harel, N. M. J. Conway, T. Yagi, J. Robertson, and W. I. Milne, J. Appl. Phys. **87**, 789 (2000).
[55]V. S. Veerasamy, J. Yuan, G. A. J. Amaratunga, W. I. Milne, K. W. R. Gilkes, M. Weiler, and L. M. Brown, Phys. Rev. B **48**, 17954 (1993).
[56]J. Schwan, V. Batori, S. Ulrich, H. Ehrhardt, and S. R. P. Silva, J. Appl. Phys. **84**, 2071 (1998).
[57]S. Waidmann, M. Knupfer, J. Fink, B. Kleinsorge, and J. Robertson, J. Appl. Phys. **89**, 3783 (2001).
[58]C. Godet, N. M. J. Conway, J. E. Bourée, K. Bouamra, A. Grosman, and C. Ortega, J. Appl. Phys. **91**, 4154 (2002).

Author complimentary copy. Redistribution subject to AIP license or copyright, see http://jap.aip.org/jap/copyright.jsp